Tuning the stress state in Nb-thin films by lateral size confinement

Philipp Klose[a,c,*], Vladimir Roddatis[b,c], Astrid Pundt[a,c]

[a] Institute for Applied Materials (IAM-WK), Karlsruhe Institute of Technology (KIT), Engelbert-Arnold-Strasse 4, Karlsruhe D-76131, Germany
[b] Helmholtz Centre Potsdam, GFZ German Research Centre for Geosciences, Telegrafenberg, Potsdam D-14473, Germany
[c] Institute for Materials Physics (IMP), University of Goettingen, Friedrich-Hund-Platz 1, Goettingen D-37077, Germany

Keywords:
Mechanical stress
Phase transformation
stress state
thin film
phase stability

A B S T R A C T

For 5 nm thin Nb films adhered to a rigid substrate, hydrogen absorption leads to ultrahigh mechanical stress of about -8 GPa. This is related to a purely elastic behaviour. The high mechanical stress destabilizes phases and even suppresses conventional two-phase regions known for the Nb-H bulk system. These unique thin film properties can be preserved to thicker films, by lateral confinement. Nb-Fe films provide a laterally confined columnar domain structure of well-separated α-Nb(Fe) and μ-FeNb phases. While the α-Nb(Fe) absorbs hydrogen at low chemical potentials, the μ-FeNb phase does not, separating the two phases into a hydrogen active and a hydrogen passive one. The behaviour of 75 nm Nb-Fe films was studied by *in situ* mechanical stress measurements, *in situ* x-ray diffraction and transmission electron microscopy. With increasing Fe-content, Nb-Fe films show a strong increase in the yield stress upon hydrogen absorption. This allows for an extended elastic range and high maximum stress values of -4.6 GPa, for 75 nm Nb-Fe films. X-ray diffraction pattern collected upon hydrogen loading of Nb-Fe films show peak shifts and intermediate peak broadening. This indicates the presence of a two-phase region and preservation of the lattice coherency between the α-Nb(Fe)-H phase and the hydride phase. Peak shifts indicate a reduced vertical expansion of the hydrogen absorbing α-Nb(Fe) lattice. This is attributed to the presence of the μ-FeNb phase. FEM simulations on Nb-Fe-H films confirm reduced overall expansions and lateral stresses, when compared to pure Nb-H films. High vertical stresses arise upon H-loading due to the link between the two Nb-Fe phases. These stresses are tensile for μ-FeNb and compressive for the α-Nb(Fe) domains and also reach values of several GPa. Conservation of the exceptional thin film properties to thicker films by lateral confinement is suggested to be a powerful strategy for many different applications like sensor technologies or energy storage.

1. Introduction

Very high mechanical stresses can be generated by hydrogen absorption in a material when it is adhered to a rigid substrate. This is due to the hydrogen-induced lattice expansion which is hindered by the substrate[1–4]. Recently, it was shown that this leads to exceptional physical behaviour. Niobium (Nb) films with a very low film thickness $h_F < 5$ nm can yield hydrogen-induced stresses of up to -8 GPa without any plastic deformation [5]. The Nb-H films behave linear elastically for the full hydrogen absorption cycle from zero to one hydrogen atom per niobium atom (H/Nb) and in reverse. In this thickness range, the common phase transformation between the α-Nb-H phase and the hydride phase is suppressed and vanishes at room temperature (RT)[6,7]. This suppression can be explained by a contribution of mechanical stress to the chemical potential [6]. If the Nb-film thickness is larger, 8 ± 2 nm $< h_F < 15\pm2$ nm, plastic deformation occurs between the film and the substrate. It reduces the mechanical stress. However for this thickness, the phase transformation still remains suppressed.

For slightly thicker Nb-films of 15 ± 2 nm $< h_F < 37\pm2$ nm, phase transformation is observed at RT in Nb-H [6]. The phases coherently match, meaning that the lattice planes between the two phases are linked. Coherency and phase transformation were verified e. g. by scanning tunnelling microscopy (STM) and X-Ray diffraction (XRD). Via STM, Nörthemann [8] and Burlaka et al. [9–11] detected hydrides[1] in the film by surface corrugations. In the coherent two-phase region, XRD-experiments show peak shift and intermediate peak broadening of only one single Nb-H (110) related peak. The finding was interpreted by the presence of small

* corresponding author
E-mail address: Philipp.Klose@kit.edu (P. Klose).

[1] It should be mentioned, that this is not the conventional β-phase of the binary phase diagram. Most probably this is a tetragonally distorted β –phase or α'-phase.

hydride precipitates whose lattice is coherently matched to the niobium matrix [12].

For Nb films thicker than $h_F > 39\pm2$ nm, the nature of the Nb-H phase transformation changes to semi-coherency between the phases [11], which includes the occurrence of microstructural defects at the phase interfaces. A distinct second diffraction peak is observed in X-Ray diffractograms. In STM investigations, steeper surface steps can be observed[11–13]. Both findings can be interpreted by dislocation loops occurring at the hydride/metal interface and releasing the mechanical stress between the two phases[13].

Mechanical stress measurements during hydrogen loading of Niobium films show a trend for the onset of dislocation formation, the yield stress $\sigma_{Y,H}$[5]. $\sigma_{Y,H}$ strongly depends on the film thickness, increasing with reduced film thickness. In general, size dependencies of the yield stress σ_Y are described by the Hall-Petch-relation[14]. This relation is valid for micro- or nano-crystalline bulk materials and not directly applicable for the case of thin films, that possess columnar grain microstructure or even epitaxial domains [14–17]. Venkatraman et al. [18, 19] distinguishes between the contributions of the film thickness (σ_{H_F}) and the lateral domain (or grain) size in a thin film system (σ_{GS}) [18–20]:

$$\sigma_Y = \sigma_{h_F} + \sigma_{GS} = \sigma_{h_F} + \frac{k}{d^n} \tag{1}$$

with d, the lateral grain or domain size and k being a constant, comparable to the Hall-Petch constant. The exponent n is material-dependent, as are all the other factors, and can take any value in the range between 0.5 and 1. As we use only one film thickness here, this contribution is set to σ_{H_F}.

In the present paper we demonstrate how to preserve the exceptional physical behaviour for Nb films thicker than $h_F = 5$ nm. According to Equ.1 it should be possible to increase the yield stress in a thin film via the lateral domain size. For films of the same thickness, the yield stress should be higher when reducing the lateral size of the domains. We here influence the lateral domain size by Fe-alloying of the Nb film. According to the bulk binary phase diagram [7], alloying Nb with Fe opens up a two-phase region containing a μ-FeNb phase in equilibrium with α-Nb(Fe). The iron-content in this α-Nb(Fe) is ofthe order of 1at%, therefore we will name it as the Nb phase. In this two-phase region, the α-Nb(Fe) volume fraction depends on the Fe-content according to the lever-rule. We examine the microstructure, the lateral stress in the α-Nb(Fe) and in the total film and, as well, the thermodynamical behaviour upon hydrogen loading. We demonstrate that the yield stress $\sigma_{Y,H}$ can be strongly increased by the presence of a passive phase via the increase of the Fe-content. We also observe a decreased stability of the hydride phase, caused by the ultrahigh mechanical stresses.

2. Experimental Details

All samples in this study were deposited on sapphire Al_2O_3 substrates ($< 0.1°$ miscut, epi-polished (CrysTec); these substrates possess very flat and smooth atomic planes on the substrate-surface). The substrates were a-plane oriented, so that the out-of-plane orientation was (11-20). One side of the substrate was parallel to the c-axis [0001]. The epitaxial relation yields the Nb films to grow with (110) directions out-of-plane and [111] planes parallel to the c-axis of the substrate.[21–24] For stress measurements, substrates of 7 mm x 30 mm x 0.1 mm size were used to achieve proper stress values via Stoney's formula. For *in-situ* X-Ray diffraction measurements and TEM studies substrates of 10 mm × 10 mm × 0.5 mm were used. To achieve equal film properties for *in situ* XRD and *in situ* stress measurements, the films were simultaneously sputtered on both types of substrates, in one sputter run.

The thin film deposition was carried out by cathode beam sputtering in an ultra-high vacuum (UHV) apparatus (fabricator: BESTEC) with a background pressure of 10^{-8} Pa. The sputtering pressure was 4×10^{-2} Pa of Argon (99.9999% purity). Growth rates were about 1.5 nm/min to 1.6 nm/min. The Nb target is of 99.99% purity. The Fe content in the films was adjusted by co-sputtering Iron (<99.95% purity). Variation of the Fe-content is carried out by placing an Fe-plate of the respective size on the Nb target. By varying the relative amount of sputtered Fe, the overall Fe content in the film and the lateral domain size can be adjusted: In a preliminary work it was found, that a columnar Nb-domain structure is formed upon co-sputtering of Nb with stainless steel, with two well-separated phases [25]. We detect the same growth mode for the Nb-Fe binary material system. The Fe-plate was suspended on a chain from the substrate holder. By this method, the size of the Fe-plate can be varied during sample transfer without opening the UHV sputter system for target exchange.

The films were sputtered at substrate-temperatures between 750°C and 800°C. In this temperature range pure Nb grows epitaxially on Al_2O_3 [6,8]. Further, the high temperature facilitates the formation of the μ-FeNb phase.

A palladium (Pd) capping layer was added after the sample was cooled down to ambient temperature. This layer enables subsequent hydrogen loading of the films and protects them from oxidation. Slight co-sputtering of Fe during the deposition of Pd is unavoidable even though the Fe-plate was placed on the outside edge of the Pd target. As the palladium capping layer only serves as a catalyst and as a barrier to prevent oxidation, a low iron content does not influence its function. In previous works it was shown, that even for higher iron-contents the catalytic feature of palladium seems to be unaffected [25,26].

The epitaxial relation between the Nb-Fe films and the substrates was studied by measuring X-Ray diffraction pole figures, on thicker films. The epitaxial relation between the Nb(Fe) domains and the Sapphire was verified. However, varying qualities of the epitaxial growth and some weak fiber texture components were observed, especially for the samples with lower Fe-content. The initial film thicknesses were determined by using X-Ray Reflectometry (XRR) (Bruker Discovery D8 with $CuK_{\tilde{\alpha}}$-radiation). High accuracy in the measured film thickness is crucial to allow precise stress and hydrogen-concentration calculations. Moreover, these examinations also displayed information about the interface roughness of all studied layers. The evaluation of the XRR-scans was carried out using LEPTOS™ (Bruker AXS GmbH: LEPTOS™ 7.7, X-Ray Data analysis software).

The films were electrochemically loaded with hydrogen in an acidic phosphorous electrolyte. The electrolyte was a mixture of one part of 85% phosphoric acid and two parts of 85% glycerine. [27] Faradays Law can be utilised to calculate the achieved hydrogen concentration in dependence of the applied electrical charge Q:

$$\Delta c_H = \frac{\Delta n_H}{n_M} = \frac{Q}{F}\frac{V_m}{V_S} \tag{2}$$

Here, V_m is the molar volume of niobium, V_s is the total volume of the thin film, and F = 96485 C/mol represents Faradays constant. The electrode potential was measured in reference to an Ag/AgCl-electrode (Schott Instruments GmbH), during all *in-situ* loading experiments. Continuous hydrogen loading was performed in case of the *in-situ* stress measurements, for all other measurements stepwise loading was used.

The content of the μ-FeNb precipitate phase was determined by using the electrode potential curves. For pure Nb films the total film volume $V_s = h_F$ A (A is the exposed film area) is used for the calculation of Δc_H in Eq. (2). As the μ-FeNb phase in the Fe-Nb films does not absorb hydrogen in a considerable amount, adjust-

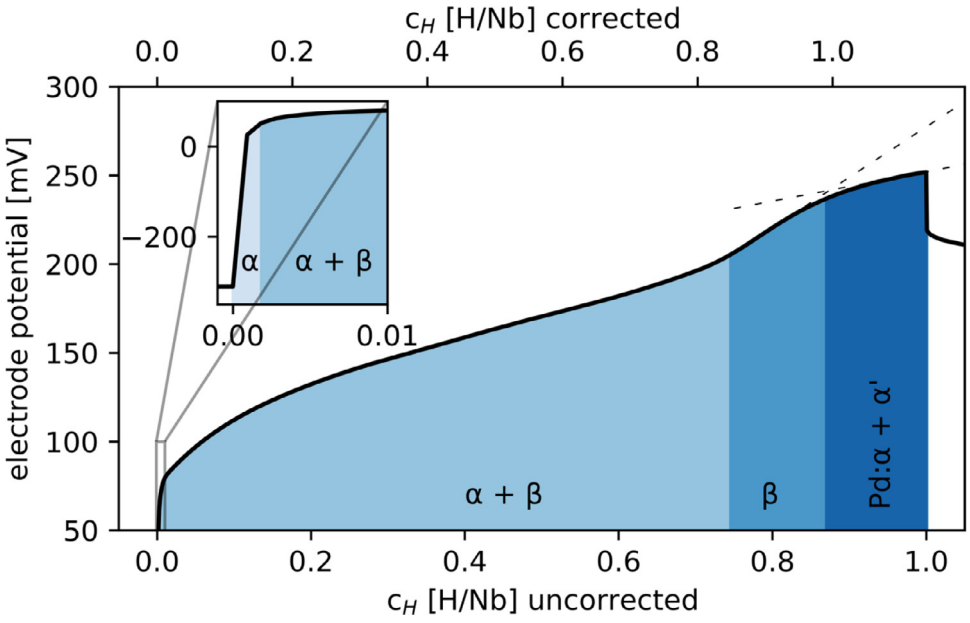

Fig. 1. Exemplary electrode potential curve in constant current loading conditions of a thin Nb film, containing about 13 Vol% of μ-FeNb. The thin, dashed lines (- - -) highlight the rescaling procedure. The occurring phase separations are highlighted by coloring and the respective labels.

ing $\Delta c_H = 1$ H/Nb leads to over-loading. This is detectable by the measured potential and serves for determining the µ-FeNb content. Subsequently, the loading curves were corrected for this µ-FeNb content [14]. This procedure will be demonstrated in the following.

Fig. 1 shows a typical potential-curve recorded during constant current hydrogen loading of a Nb-Fe film. The constant current loading condition leads to a noticeable offset between the measured and the equilibrium electrode potential. In equilibrium-conditions, the electrode potential for the α-Nb-H and β-hydride – plateau would be around 80 mV [11]. This value is close to the observed starting value, shown in Fig. 1. This confirms that the content of Fe in the Nb-regions is small. According to the bulk phase diagram it is about 2% at RT. Fig. 1 also shows an increasing potential in the two-phase region. This can be attributed to mechanical stress and furthermore, the isotherm slope here is affected by the continuous loading condition. The overpotential (that is needed for the incorporation of hydrogen into the sample) increases with increasing hydrogen concentration.

Even though, the potential-curve allows assigning the different phases forming during H loading. InFig. 1, the Nb(Fe)-H α-phase is present for small H-concentrations of up to 10%. For simplicity, the small content Fe is neglected in this graph. Increase of the hydrogen content results in phase separation between the Nb-H α-phase and the Nb-hydride phase. The Nb-hydride phase is here denoted as β. According to Fig. 1, β-phase forms for H-concentrations above 0.75 H/Nb (lower axis), or after correction above 0.82 H/Nb (upper axis). For hydrogen concentrations higher than 1 H/Nb (upper axis), the Pd capping layer is loaded, which can be determined by the two-phase region appearing at a electrode potential of about 250 mV, in the constant loading condition. The value of the electrode potential of the Pd α-α'-plateau confirms, that the Fe content in the Pd-film must be low. There is no additional plateau detected that accounts for the hydrogen loading of the µ-FeNb. This verifies, that the µ-FeNb phase does not form a hydride, for the studied potential range.

Two dashed lines are aligned parallel to the ascending β-region (blue) and parallel to the sloped palladium – palladium hydride - plateau (dark blue). The intersection between both lines is chosen to determine the concentration of Δc_H=1 H/Nb for correction, as shown in the upper axis in Fig. 1. This correction bases on the assumption that the Nb-volume loads to 1 H/Nb in spite of the small Fe content.

Hence, the volume fraction of the µ-FeNb phase can be estimated by comparing the corrected and the uncorrected concentration axes. The relative deviation of the corrected hydrogen content (upper axis) from the uncorrected hydrogen content (see lower axis), equals the relative precipitate fraction of µ-FeNb in the Nb-matrix [25]. In the shown example of Fig. 1, the precipitate fraction equals to 13%. The Nb-Fe samples exhibit volume fractions between 4 Vol% and 39 Vol% of µ-FeNb precipitate in the 96 Vol% to 61 Vol% hydrogen sorbing Nb-matrix.

For a sufficiently thin substrate, the hydrogen induced in-plane stress leads to sample curvature. The bending radius of the sample can be utilized to calculate the lateral stress by using Stoney's equation [28–30]. The hexagonal symmetry of the lattice requires some adaptations [5]. Finally, the stress change is given by

$$\Delta\sigma = \frac{M_S d_S^2}{6\, d_f}\left(\frac{1}{R} - \frac{1}{R_0}\right) \quad , \tag{3}$$

with the thicknesses of substrate d_s and film d_f, R as the radius of the curvature of the sample and R_0 the initial curvature. For the *in situ* stress measurements, the cantilever sample is mounted on one side to a rigid fixture. A capacitive displacement sensor measures the distance to a very small metal chip, which is glued to the far end of the cantilever sample. The sample curvature is calculated from the cantilever length and the height change. The whole setup is submerged in the electrolyte.

The used mean isotropic elastic modulus of the substrate is M_s= 534.5 GPa [5]. The initial curvature R_0 of the sample at the beginning of the *in-situ* stress measurement is not measured. We, therefore, only present the hydrogen-related stress changes $\Delta\sigma$. For simplicity, we artificially set the initial stress to $\sigma_0 = 0$ GPa, in the figures. However, lateral stresses are also expected for the as-prepared state.

Transmission electron microscopy (TEM)-lamellae were prepared from the samples that contain 13 Vol% and 39 Vol% of µ-FeNb precipitates, respectively. The lamella preparation was carried out using a focused ion beam (FIB) process (FEI Nova Nano Lab 600, Ga-Ion-source). To protect the sample from ion-damage

and implantation, the surface was covered with Pt. Subsequently, several milling steps were performed to produce the lamellae.

The lamellae were studied in a FEI Titan environmental (E)-TEM equipped with a C_S image corrector. For all studies, the field emission gun was operated at 300kV. For scanning (S)TEM-EELS (electron energy loss spectroscopy) a Gatan image filter was used. High-resolution micrographs were recorded to survey the films microstructure. To get insights into the elemental distribution, scanning (S)TEM-EELS mappings were performed. The analyzed EEL edges were the L-edges of niobium and iron, respectively.

All *in-situ* XRD measurements were done using the D8 goniometer (Bruker), using copper (Cu) radiation. In the case of X-Ray diffraction on the substrate-peak, peak splitting between $CuK_{\alpha 1}$ and $CuK_{\alpha 2}$ was observed. But no peak splitting of the film diffraction peaks could be observed. This is due to the small film thickness and to a distribution of the lattice parameters. Thusly, all calculations of lattice parameters of the films were done with the intensity-weighted average wavelength of $Cu_{K\bar{\alpha}}$ = 1.542 Å. Luminescence effects of the iron, irradiated by Cu-radiation were not observed, as the used LYNXEYE^{TM} detector is energy selective.

Hydrogen was offered *in-situ* by step-wise loading. After each loading step, two X-Ray diffraction scans were performed. One scan mainly contained the Al_2O_3 (11-20) peaks, the other scan is mainly used to observe the Nb-(110)-peak and the Pd-(111)-peak in greater detail. To suppress the highly intensive Al_2O_3 peaks, that would overlap the Nb-(110)-peak of the second scan, we applied a very small ω-offset of 0.04° from the ideal diffraction condition. Preceding scans revealed no ω-offset-dependence of the peak-positions in the relevant offset-range.

All peaks in the obtained scans were fitted with the Pearson-VII model. As peak shapes change during the hydrogen loading-experiments under the influence of mechanical stress during phase transformations, Pearson-VII-peaks fit all occurring peak shapes.

The sapphire peak scans were used to calibrate all performed scans according to the maximum intensity of the Al_2O_3 (11-20) Cu $K\alpha_1$ peak. The fit-results of the Nb- and Pd- diffraction intensities will be viewed in more detail, subsequently. For coherent phase transformations in Nb-H films, where no dislocations are formed at the interface between hydride-phase and metal-matrix, a temporary peak broadening can be observed upon phase transformation [31]. The full width at half maximum (FWHM) of the related peak can be utilized to determine the solubility limits [9]. For the case of semi- or incoherent phase transformations in Nb-H films, intermediate peak separation can be observed, as the lattice parameters of both phases are allowed to differ by the presence of dislocations at the interface between both phases.

The *in situ* XRD out of plane lattice expansion of the different phases will be correlated to the global *in situ* lateral stress measurements from the substrate curvature setup. The measured out-of-plane lattice expansion can further be connected to linear elastic calculations on in-plane stresses.

3. Theory

Linear elastic theory allows to evaluate the vertical expansions and lateral stresses upon hydrogen absorption in films ideally adhering to rigid substrates [32]. The situation here is more complex, as the Nb-Fe films consist of two different domains, α-Nb(Fe) and µ-FeNb. But, it is not expected that the µ-FeNb sorbs considerable amounts of hydrogen. Thus, hydrogen absorption in this phase is neglected here. By this, the α-Nb(Fe) -domains will be regarded as the active phase that absorbs hydrogen while the µ-FeNb is regarded as the passive phase. The behavior of the α-Nb(Fe) upon hydrogen absorption will be discussed in the following by assuming similar elastic constants as in pure Nb. For simplicity, we rename the low Fe-content α-Nb(Fe) phase with α-Nb phase. The effect of the presence of the µ-FeNb phase on stress and strain will be regarded in a next step, in FEM simulations.

Linear elastic theory

Bulk Nb expands linearly by a factor of $\alpha_{H,bulk}$=0.058 Δc_H [33] upon hydrogen loading to 1 H/Nb. An ideally adhering thin film poses an insuperable constraint against lateral expansion. This situation changes the expansion behavior during hydrogen absorption, so that only vertical expansion remains possible for the adhering thin film. The hindered lateral expansion also results in ultrahigh lateral stresses in the overall sample.

The maximum vertical expansion of a fully adhered pure Nb film upon hydrogen absorption can be calculated by linear elastic theory. Using the known bulk Nb elastic constants (C_{11} = 245 GPa, C_{12} = 132 GPa, C_{44} = 28 GPa at a temperature of T = 300 K [34]), the vertical expansion $\varepsilon_{zz} = \alpha_{H,film}\Delta c_H$ gives 0.136 as the expansion factor $\alpha_{H,film}$ [5,35]. The lateral stress calculates to $\sigma_{[111]}$ = -9.1 GPa c_H along the lateral [111] directions, which is the mainly measured direction of lateral stress in this work.

The out-of-plane expansion $\alpha_{H,Film}$ = 0.136 of a hydrogen loaded pure Nb film is larger than that of the free bulk Nb sample because of the adhesion to the rigid substrate. Thus, the measured vertical expansion ε_{zz} will be $\frac{0.136}{0.058} = 2.344$ times larger than the expansion of a free sample ε_0,

$$\varepsilon_{zz} = \frac{d_{(110)} - d_{(110,LIT)}}{d_{(110,LIT)}} = 2.344\ \varepsilon_0 \tag{4}$$

In this case the vertical expansion can be calculated from the measured lattice spacing $d_{(110)}$ upon hydrogen loading, using the bulk stress-free interplanar spacing $d_{(110,LIT)}$ = 2.33 Å [36]. To calculate the lateral stress along the lateral [111]-direction, which is in parallel to the long axis of the cantilever in the stress measurement setup, the vertical expansion ε_0 has to be multiplied with the stiffness $k_{[111]}$. The stiffness $k_{[111]}$ in [111] film direction was calculated following the procedures described in Ref. [37–39],

$$k_{[111]} = \frac{-C_{11}^2 - C_{11}C_{12} + 2C_{12}^2 - 10C_{11}C_{44} - 20C_{12}C_{44}}{3C_{11} + 3C_{12} + 6C_{44}} \tag{5}$$

Hence, the lateral stress along the [111]-direction is given by

$$\sigma_{[111]} = \varepsilon_0\ k_{[111]} = \frac{d_{(110)} - d_{(110,LIT)}}{2.344\ d_{(110,LIT)}}(-154.5\ \text{GPa}) \tag{6}$$

The calculation is only correct, as long as no plastic deformation takes place. Certainly,the two-phase situation of the Nb-Fe films containing α-Nb(Fe) and µ-FeNb is more complex. However, the local lateral stresses in the Nb(Fe)-H domains can be derived from the vertical lattice spacing detected by XRD on the Nb(Fe) (110)-lattice reflection [6], by using Eq. (6). Again, the small Fe content in α-Nb(Fe) is neglected, as well as the presence of other domains.

Finite element method (FEM) simulations

To model the complex situation of the two adjacent phases, 2D Finite-Element simulations were performed using the commercial Comsol Multiphysics® Modeling software (version 5.2). The solid mechanics module was used to simulate stress and strain (displacement) in the cross-section of a thin film. In this case, the hydrogen induced expansion of the material was modeled as a thermal expansion of the niobium phase, because all underlying mathematics and symmetries are analogous. For this procedure the thermal expansion coefficient of the material is adjusted to the hydrogen induced expansion coefficient (as discussed above) and the temperature of the system is artificially increased from 0 K to 1 K. This equates the hydrogen loading from 0 to 1 hydrogen per niobium atom.

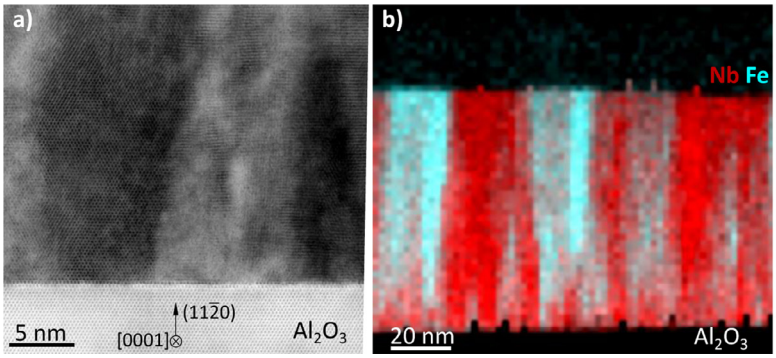

c) Domain sizes in nm

	Nb	*μ-FeNb*
13 Vol%	**50**	**10**
39 Vol%	**15**	**25**

Fig. 2. STEM micrographs **a)** STEM-BF image to highlight the unique microstructure of the prepared Nb-Fe thin film samples, containing 39 Vol% of μ-FeNb. The darker area relates to Nb with an (110)-out of plane orientation. This phase is semicoherently matched to the μ-FeNb phase, visible with lighter contrast. **b)** STEM-EELS color mapping image of the relative elemental distribution of Niobium (red) and Iron (cyan). Regions of pure Fe were not observed. Fe only occurs in conjunction with Nb. On the other hand, deep red areas highlight pure Nb domains **c)** measured lateral domain sizes of the Nb- and μ-FeNb-domains

4. Results

Fig. 2 provides high-resolution STEM-BF (bright field) images and a STEM-EELS map of a Nb-thin film sample containing 39 Vol% of μ-FeNb. In Fig. 2a), the Nb-phase appears in darker contrast and the μ-FeNb domains appear with brighter contrast. They are aligned in a columnar arrangement, with lateral extensions of about 10-15 nm in the shown frame. Fig. 2b) shows a STEM-EELS image where red (Nb) and cyan (μ-FeNb) encode the presence of the different elements. The EEL-spectra exclude the presence of pure Fe regions, as no pure Fe signatures were found in the underlying spectra. The STEM-EELS maps verify the phase separation between Nb and an Fe- and Nb-containing phase. The columnar arrangement of the Nb-containing phase and the Fe and Nb containing phase are visible. Mixed color regions originate from columns overlap.

The STEM-EEL spectra also provide insight into the phase fractions via the elemental composition. These phase fractions agree very well with the electrode potential results according to Fig. 1. We assume a relative error of about ±10% for the STEM EELS phase fraction.

Fig. 2a) further highlights the mainly coherent interface between the Nb- and μ-FeNb domains. Upon further examination of the STEM-micrographs by fast Fourier transform (FFT), the presence of single dislocations between niobium and the precipitate phase becomes apparent. We expect the central α-Nb-region to behave differently to the interface-region, due to the link to the non-sorbing μ-FeNb phase[40].

Lateral domain dimensions were measured for both samples, on a larger scale, and summarized in the table in Fig. 2c).

Electrochemical hydrogen loading was performed on the Nb-Fe films. The lateral mechanical stresses were measured *in-situ* utilising the substrate curvature method. On selected samples *in-situ* XRD experiments were carried out, in which diffraction scans were performed after small incremental hydrogen loading steps. The methods allow measuring the lateral stresses, as well as the vertical lattice expansion.

Fig. 3 shows the hydrogen induced lateral stress increase of three films of 75 nm thickness which differ in their μ-FeNb precipitate content between 4 Vol% to 39 Vol%. The characteristics are summarized in Table 1. All stress curves start off with a linear elastic regime, the stress increase of all samples is between -4.6 GPa c_H and -6.8 GPa c_H. All of these values are significantly smaller than that of the hydrogen loaded Nb-films. There, the stress increase mainly depends on the crystallographic orientation of the film. For the (110)[111]-orientation of the Nb film, -9.1 GPa c_H is expected according to linear elastic theory. This orientation relation is also found for the niobium phase in the Nb-Fe films.

Table 1
The table contains the characteristics of the stress measurements provided in Fig. 3: the linear stress increase at small H-concentrations, the onset of plastic deformation described by the critical concentration $c_{H,Y}$ and the related yield stress $\sigma_{H,Y}$.

precipitate fraction [Vol%]	stress increase in linear elastic regime [GPa c_H]	Critical concentration $c_{H,Y}$ [H/Nb]	stress $\sigma_{H,Y}$ [GPa]
4 (—)	-4.6	0.26	-1.22
13 (- - -)	-6.8	0.5	-3.37
39 (---)	-5.6	0.86	-4.39

Texture measurements revealed trace amounts of fibre texture components in the samples. Notably, the relative fraction of the fibre texture component decreases with increasing precipitate content, respectively the iron content. This observation matches to the stronger stress increase measured for the films, that exhibit a better quality of the epitaxial growth relation. The fibre texture components relate to nanocrystalline film volumes, that are expected to possess a lower stress increase because of the presence of grain boundaries.

The linear elastic regime, where the measured stress increases linearly, is broader in hydrogen concentration for increasing relative precipitate content. According to Tab.1, it ends at 0.26 H/Nb for the 4 Vol% containing film and ends at 0.86 H/Nb for the 39 Vol% containing film. Hence, the plastic deformation is shifted to higher stresses and higher hydrogen concentrations for higher precipitate volume contents and, in turn, for smaller lateral niobium domain sizes.

If the measured stress were purely related to the niobium-H volume content, an effective lateral stress can be calculated. For the 39 Vol% containing Nb-Fe sample, the total Nb-H fraction is 61 Vol% and the linear elastic stress increase is – 5.6 GPa, thus

$$\Delta\sigma = \frac{-5.6\ \text{GPa} \cdot c_H}{0.61} = -9.2\ \text{GPa} \cdot c_H \qquad (7)$$

This value matches the theoretical calculation of the hydrogen-induced stress of - 9.1 GPa, in this lattice direction. This shows the influence of the Nb itself and verifies the passive behaviour of the μ-FeNb phase. It gives the hydrogen-related stress increase as introduced by the active Nb-phase.

Fig. 4 shows the diffraction pattern of an in-situ X-Ray diffraction experiment during hydrogen loading of a 75 nm thin Nb-Fe film that contains 39 Vol% of μ-FeNb. It focusses on the 2θ-range

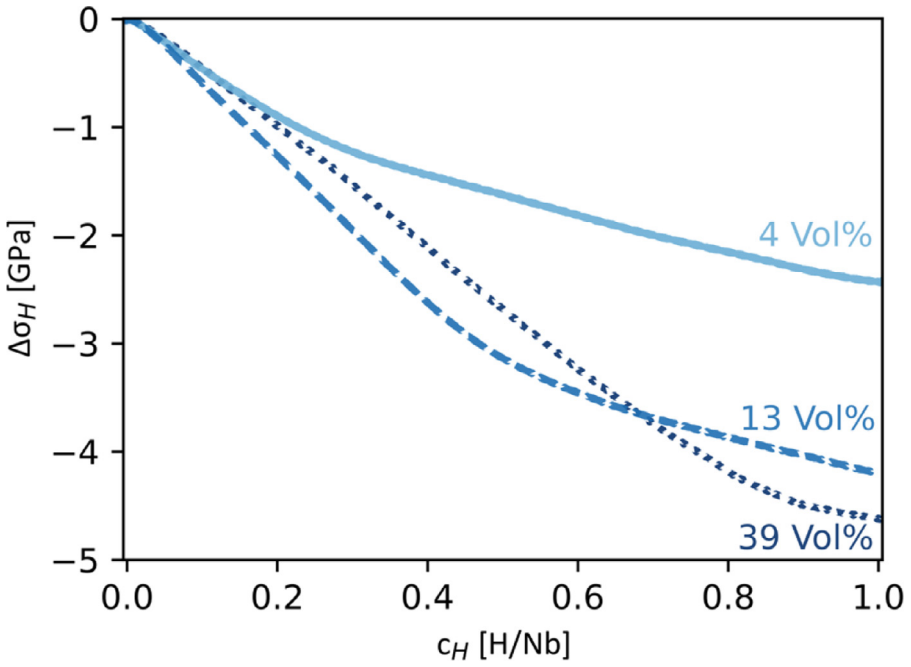

Fig. 3. Stresses arising during H-loading in 75nm thin films with different μ-FeNb precipitate contents, as measured by the substrate curvature method. Increasing the precipitate content in the film increases the final stresses.

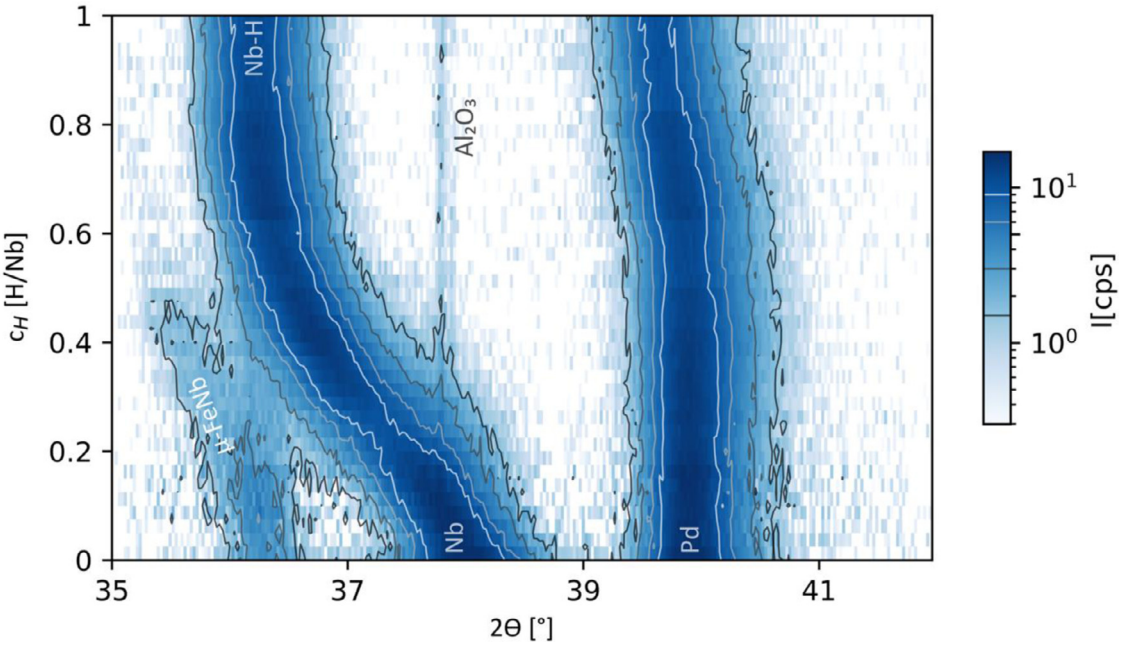

Fig. 4. In-situ X-Ray diffraction experiment during hydrogen loading of a 75 nm thin Nb-Fe film, containing 39 Vol% of μ-FeNb. The experiment was carried out using a self-designed *in-situ* cell for electrochemical loading in a Bruker D8 using Cu-$K_{\bar{\alpha}}$-radiation. Three peaks are detected related to (111)-Pd, (110)-Nb, and (110)-FeNb. The diffraction condition is tilted to 0.04° from the ideal Bragg condition to suppress the intensive Al_2O_3 substrate peaks, their remnants are still visible at $2\theta = 37.7°$.

between 35° and 42°. The vertical axis gives the hydrogen concentration in the Nb domains (for more information see Fig. 1 and accompanying text) while the peak intensity is color-coded. For the initial state, separated peaks are detected for the (110) Nb at $2\theta = 37.9°$, for the (111) Pd cover layer at $2\theta = 39.9°$ and at about $2\theta = 36.3°$. This weak peak appears at the expected position of the (110)-μ-FeNb diffraction peak. It supports the formation of the μ-FeNb phase expected from the bulk phase diagram, also in the thin film. The position of the (110) Nb shifts to lower angles with increasing hydrogen content. No separated new Nb-hydride peak is observed. A shift is also visible for the (110)-μ-FeNb diffraction peak. The (111) Pd peaks starts shifting above 0.6 H/Nb. This is mainly related to the H-absorption in the Pd α-phase.

The shift of all peaks is presented in Fig. 5a), as function of the hydrogen content in the Nb domain between 0 and 1 H/Nb, and on the related lattice parameter. The corresponding in-plane stress in the Nb-volume, as calculated by using the peak shift of the (110) Nb-peak via Eq. (6), is plotted in Fig. 5b), as function of the hydrogen concentration. Also implemented in Fig. 5b) is the mean stress of the complete sample, which was measured by the substrate curvature method (see Fig. 3). As can be seen in Fig. 5b), the stress evolution upon hydrogen loading first develops equally

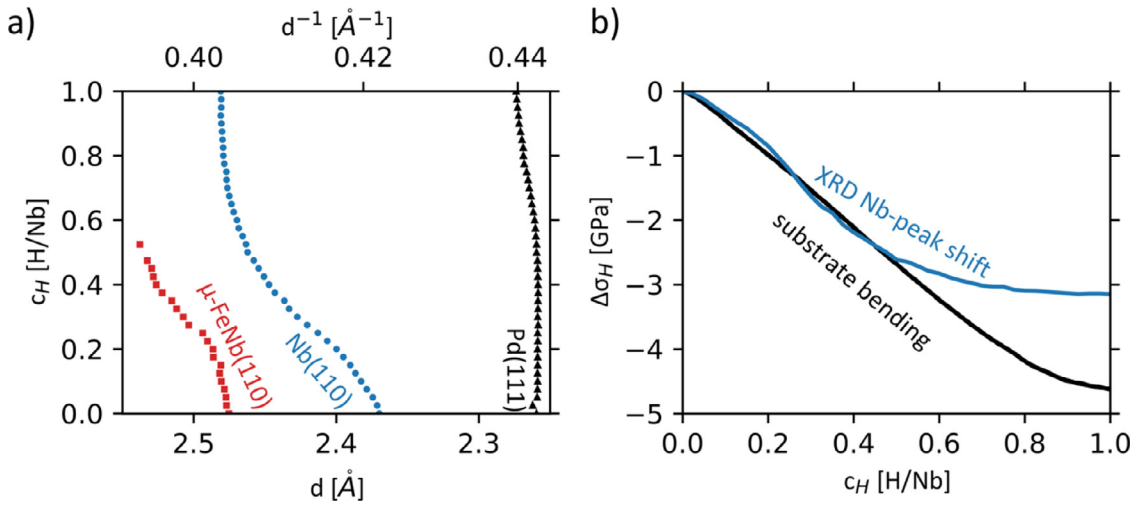

Fig. 5. a) Peak shift during the hydrogen absorption of the 75 nm thick Nb film, which contains 39 Vol% of μ-FeNb. During the loading of the sample, the Niobium (blue circles •) and Ferroniobium (red squares ■) expand vertically. For higher concentrations, the Palladium (black triangles ▲) also shows a slight vertical lattice expansion. **b)** The Nb-110-peak shift was recalculated to lateral stresses that are necessary to generate the observed vertical lattice expansions according to linear elastic theory. This resulting stress is compared to the mean stress that was measured by the substrate bending technique.

on the hydrogen concentration in the Nb domain, for both methods. But for higher hydrogen concentrations $c_H > 0.5$ H/Nb, the stress evolution originating from the peak shift suggests lower lateral stresses in the niobium domains compared to the stress measured by substrate bending. The final stress only reaches -3.1 GPa as determined from the diffraction peak position, but -4.6 GPa as determined by substrate bending. We interpret this difference by the presence of the passive phase. It is expected that the vertical expansion of the Nb volumes in the film, detected by XRD measurements, is affected by this phase. Certainly, it also affects the total lateral stress, as measured by substrate curvature. The influence of the passive phase on the stress and strain is addressed by FEM simulations.

The intermediate peak broadening of the Nb(110)-peak and the lack of a second Nb-H-peak indicates coherent phase separation in the Nb domains, during H-loading. This can be seen in Fig. 4 between diffraction angles of 37° and 38° and in the concentration range between 0.15 H/Nb and 0.25 H/Nb.

FEM simulations and discussion

FEM simulations were performed to describe the observed stress and strain development in the heterogeneous two-phase films upon hydrogen loading. A simple model was designed to mimic the observed microstructure in 2 dimensions (2D), as shown in Fig. 6. The bottom line is fixed, accounting for the adhesion to the rigid substrate. The left and right sides are configured with periodic boundary conditions, so that all forces that exert these sides affect the opposing side. This effectively reproduces an infinite amount of Nb domains aligned next to each other, separated by the μ-FeNb domains. In the simulations, the initial film thickness is set to 75 nm.

The respective lateral and vertical stresses of the different lateral domain sizes were investigated, as well as the vertical displacement. The (relative) vertical displacement should be similar to the lattice expansion that is measured by the peak shift in X-Ray diffraction experiments.

The following results are used to illustrate the situation of mechanical stress, they were calculated using isotropic elastic conditions. Therefore, the results will yield guidelines for the understanding of the lateral and vertical stress states and the resulting lattice expansion in thin film samples of this unique microstructure.

Different lateral domain sizes have been modelled, the examples shown in the upcoming figures mainly show the samples of 13 Vol% and 39 Vol% precipitate content. Their respective domain sizes were measured from the TEM images as shown in Fig. 2c). The meshing used to simulate the system was set to 'extremely fine', as shown in Fig. 6b). No effects due to the meshing size could be observed, only for very coarse and manual meshing. Thus, the meshing has no influence on the simulation results, in the provided examples.

Figs. 7 and 8 represent stress mappings of the samples that contained 13 Vol% and 39 Vol% of precipitates, respectively. Fig. 7 shows compressive stresses in the lateral direction for all shown phases and domain size combinations. In the vertical direction, the μ-FeNb phase (assigned as FeNb) is under tensile stress, while in turn the Niobium phase (assigned as Nb) is under vertical compressive stress.

The larger the niobium domain is compared to the FeNb domain, the higher are the resulting vertical forces, as is represented by the size of arrows in Fig. 7. The vertical expansion of the niobium phase is obstructed.

Both Figs. 7 and 8 show the reduced lateral stress by the presence of the passive μ-FeNb-Phase. The larger the precipitate content, the higher is this reduction and the higher the counteracting vertical stresses are. The colored surface plot of Fig. 8 also shows the resulting shape of the domain after hydrogen loading to 1 H/Nb in respect to the initial state, which is marked by the thin black lines.

In the same surface plot, we can see the overall reduction of vertical expansion, followed by the ultrahigh vertical stresses that arise in the domains. This reduction of the vertical displacement of the Nb phase matches the reduction of lattice expansion, as it was observed by XRD in Fig. 5b). There exists a strained interface region between the active and the passive phase. We assume that this region solves hydrogen in a different way and might not contribute to the Nb-H α-phase reflection or to the μ-phase reflection. This concentration change in the interface region is not included in the FEM calculations. It might explain the deviation of the stress values for the two different methods in Fig.5b), occurring at H/Nb > 0.5 H/Nb. We may also include a slight absorption of hydrogen

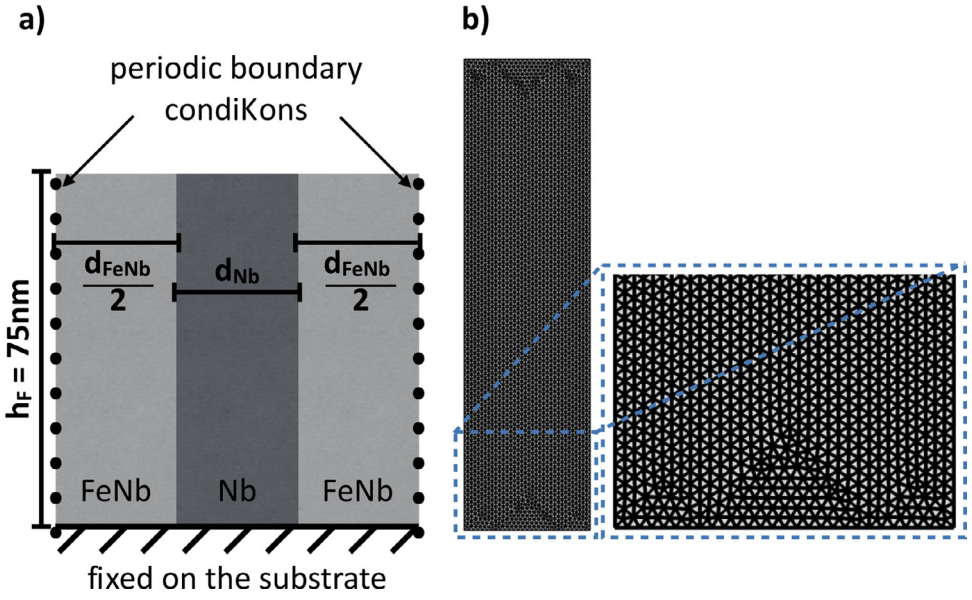

Fig. 6. Schematic drawings of the arrangement used in the FEM-simulations to calculate stresses and displacement. **a)** Periodic boundary conditions are used, so that the forces that exert the left and right side, affect the other side. The bottom edge is fixed to the rigid substrate. The initial film thickness is set to 75 nm, the lateral domain sizes d_{FeNb} and d_{Nb} are varied between 5nm and 50 nm, with increments of 5 nm. **b)** meshing of the model with detailed view

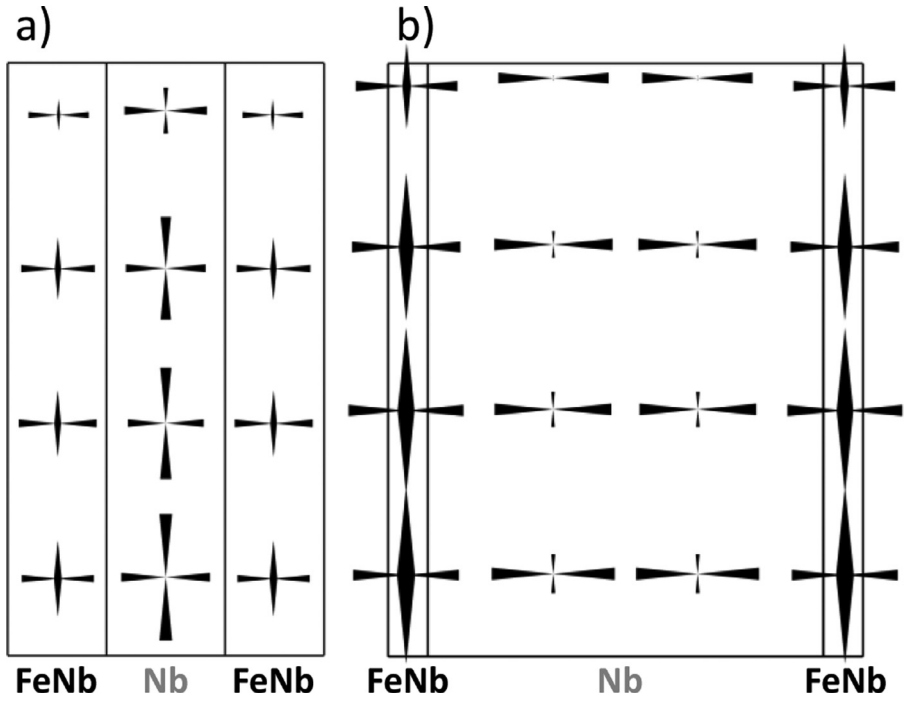

Fig. 7. Symbolic description of resulting stresses of both domains. The size of the arrows correlates to the magnitude of the arising stresses both in lateral (horizontal cones) and vertical directions (vertical cones). If the cones point towards each other, the stress is compressive, if they point away from each other, the corresponding stress is tensile. The FeNb domains are under tensile stress vertically, whereas the Nb is in a compressive stress state. All domains show high lateral stresses. The lateral domain sizes are respective to the 39 Vol% (a) and 13 Vol% (b) samples with the measured domain sizes of Fig. 2c).

in the μ-FeNb phase. This is planned to be addressed in a forthcoming study.

The simulations also reveal modulations of the lateral stress between both phases. The lateral compressive stress in the niobium domains is lower than in the μ-FeNb domains. The amplitude of this modulation is about 500 MPa in case of the studied domain sizes and resembles a sinusoidal curve. Lateral stress modulations are not seen in the substrate curvature stress measurements as they only provide the global stress. These modulations should lead to an increase of the peak width of the Nb-diffraction peak towards the end of the in situ loading experiment. Indeed, such an effect is observed for the 13 Vol%- film. In the case of the 39 Vol%-film, this effect is not visible, presumably due to the stronger stabilisation effect of the surrounding μ-FeNb domains. The vertical stresses are counteracting between both domains, as the niobium domain expands vertically, which forces the μ-FeNb to expand vertically as well. This leads to compressive vertical stresses in the niobium domains (red) and tensile stresses in the μ-FeNb phase (blue), as can be seen in Fig. 8.

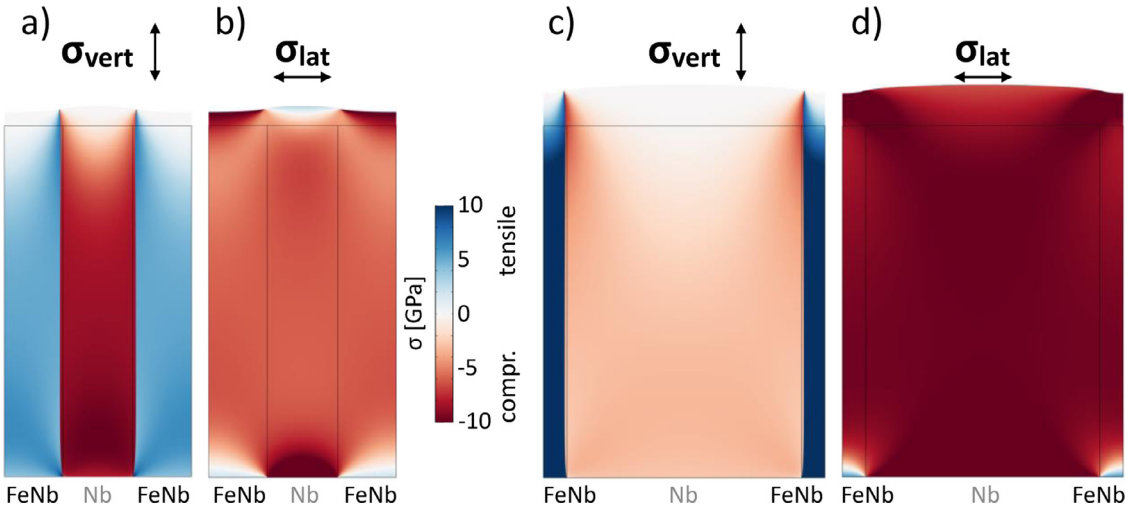

Fig. 8. Combined surface plots of vertical (a and c) and lateral (b and d) stresses, as calculated by FEM-Simulations (Comsol Multiphysics® 5.2; solid mechanics module). The diverging color-scale highlights the tensile (positive, blue) stress in the μ-FeNb domains and the compressive vertical stresses in the niobium domains that arise as a result of the lattice coherency between both phases. Resulting from this, lateral stress varies between both domains with an amplitude of about 500 MPa.

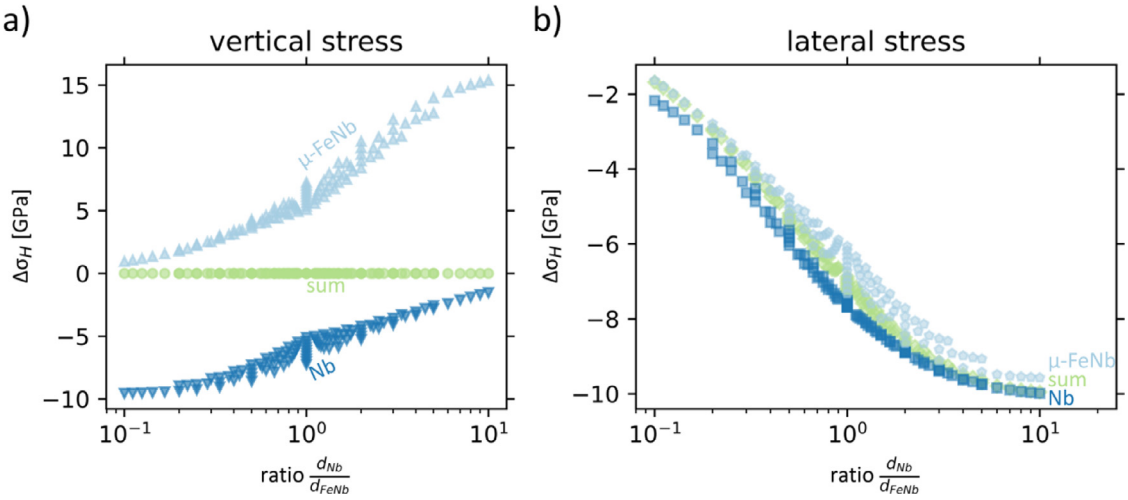

Fig. 9. Dependence of the resulting lateral and vertical stresses of the respective domain size ratios. The presence of the passive μ-FeNb-phase leads to a reduction of the overall lateral stress upon generation of opposite vertical stresses.

The magnitude of the lateral stress change can be influenced via the ratio of Nb and μ-FeNb domains sizes, as can be seen in the difference between Figs. 7 a) and 7 b) and 8 a),b) and c),d). The overall measured lateral stress also decreases, for a lower relative niobium content.

In situ X-Ray diffraction experiments reveal the nature of the phase separation during the hydrogenation of the niobium. All alloyed films of 75 nm show intermediate peak broadening, which indicates a coherent phase separation, within the Nb domains. This differs from pure Nb films, where the coherent phase transformation was only detected for pure Nb-H films thinner than $\geq 39 \pm 2$ nm [31], thicker films show semi-coherent phase transformation (e.g. by peak-splitting of the α-Nb and the Nb-hydride peak). This change of the nature of the phase transition is probably linked to the change in the stress state of the niobium domains themselves. Additionally, the vertical expansion of the niobium lattice is reduced greatly by the presence of the μ-FeNb precipitate phase.

Thus, the FEM simulations reveal a lowered overall expansion for the studied lateral domain sizes. Due to coherent matching between the Nb and the μ-FeNb domains, a unique stress state arises during the hydrogen loading. The niobium domain has to expand vertically. The surrounding μ-FeNb follows this vertical expansion. This can be directly seen in the XRD pattern in Fig. 4 by the shift of the Nb and the μ-FeNb lattice reflections. Due to the very high lateral compressive stresses and also the transverse strain of the precipitate phases, the Nb is allowed to slightly expand laterally. Thereby, high lateral stresses of several GPa are generated in both phases, with only around 500 MPa of modulation. On top of this, also high vertical stresses arise in both domains: The μ-FeNb is under tensile stress, as it is stretched by the expanding Nb domains. In turn it compresses the Nb domains in vertical direction. These vertical stresses also reach values of several GPa, a situation that is highly different from single phase adhered films. Fig. 9 can be used to adjust the desired hydrogen-induced stress state in the sample by the choice of the phase ratio of μ-FeNb and Nb. It serves as an example for the possible stress modification by combining active and passive phases.

Conclusions

The presented work demonstrates that the mechanical stress development and also the thermodynamic behaviour of materials can be controlled by modification of the constraint conditions, e.g. the lateral domain size and the coherency state between these

domains. By the lateral constraint condition we achieve about 20 times larger critical film thicknesses of plastic deformation than previously reported for Nb films[5]. This allows for ultrahigh linear elastic mechanical stresses while maintaining coherent phase boundaries between the hydride, its host metal lattice and the μ-FeNb precipitate phase. This suggests that beneficial properties of nano-size systems can be preserved for larger scales by lateral micro-structuring. This concept is relevant for all those systems where ultrahigh mechanical stress, modified thermodynamics or purely elastic and reversible behavior are of interest, for example in intercalating energy storage materials such as metal-hydride storage systems or Lithium ion battery technologies.

Declaration of Competing Interest

The authors declare that they have no known competing financial interests or personal relationships that could have appeared to influence the work reported in this paper.

Acknowledgements

Financial support of the Deutsche Forschungsgemeinschaft (DFG) via PU 131/9-2 and PU 131/12-1 is gratefully acknowledged. Volker Radisch is explicitly thanked for the focused ion beam TEM sample preparation.

References

[1] G. Song, a. Remhof, K. Theis-Bröhl, H. Zabel, Extraordinary Adhesion of Niobium on Sapphire Substrates, Phys. Rev. Lett. 79 (1997) 5062–5065, doi:10.1103/PhysRevLett.79.5062.
[2] G. Song, M. Geitz, A. Abromeit, H. Zabel, Solubility isotherms of hydrogen in epitaxial Nb(110) films, Phys. Rev. B. 54 (1996) 14093–14101, doi:10.1103/PhysRevB.54.14093.
[3] G. Song, A. Remhof, D. Labergerie, C. Sutter, H. Zabel, Hydrogen in thin epitaxial Nb films, J. Alloys Compd. 293–295 (1999) 476–479, doi:10.1016/S0925-8388(99)00468-5.
[4] L. Schlapbach, Hydrogen in intermetallic compounds I, Electronic, thermodynamic, and Crystallographic Properties, Preparation (1988) https://link.springer.com/978-3-540-47882-9. accessed March 8, 2019.
[5] M. Hamm, V. Burlaka, S. Wagner, A. Pundt, Achieving reversibility of ultrahigh mechanical stress by hydrogen loading of thin films, Appl. Phys. Lett. 106 (2015) 243108, doi:10.1063/1.4922285.
[6] V. Burlaka, S. Wagner, M. Hamm, A. Pundt, Suppression of Phase Transformation in Nb–H Thin Films below Switchover Thickness, Nano Lett 16 (2016) 6207–6212, doi:10.1021/acs.nanolett.6b02467.
[7] T. Massalski, H. Okamoto, P. Subramanian, Binary alloy phase diagrams (1986).
[8] K. Nörthemann, R. Kirchheim, A. Pundt, Surface modification of Nb-films during hydrogen loading, J. Alloys Compd. 356–357 (2003) 541–544, doi:10.1016/S0925-8388(02)01259-8.
[9] V. Burlaka, S. Wagner, M. Hamm, A. Pundt, Suppression of Phase Transformation in Nb–H Thin Films below Switchover Thickness, Nano Lett 16 (2016) 6207–6212, doi:10.1021/acs.nanolett.6b02467.
[10] V. Burlaka, S. Wagner, A. Pundt, In-situ STM and XRD studies on Nb–H films: Coherent and incoherent phase transitions, J. Alloys Compd. 645 (2015) S388–S391, doi:10.1016/J.JALLCOM.2014.12.103.
[11] V. Burlaka, Critical thicknesses in Nb-H thin films: coherent and incoherent phase transitions, change of precipitation and growth modes and ultrahigh mechanical stress, Georg-August-Universität Göttingen, 2015 https://opac.sub.uni-goettingen.de/DB=1/FKT=1016/FRM=Vladimir%2BBurlaka/IMPLAND=Y/LNG=DU/LRSET=1/SET=1/SID=24243fd5-4/SRT=YOP/TTL=1/SHW?FRST=1 (accessed October 12, 2018).
[12] V. Burlaka, S. Wagner, A. Pundt, In-situ STM and XRD studies on Nb–H films: Coherent and incoherent phase transitions, J. Alloys Compd. 645 (2015) S388–S391, doi:10.1016/J.JALLCOM.2014.12.103.
[13] K. Nörthemann, A. Pundt, Coherent-to-semi-coherent transition of precipitates in niobium-hydrogen thin films, Phys. Rev. B. 78 (2008) 014105, doi:10.1103/PhysRevB.78.014105.
[14] E.O. Hall, The Deformation and Ageing of Mild Steel: III Discussion of Results, Proc. Phys. Soc. Sect. B. 64 (1951) 747–753, doi:10.1088/0370-1301/64/9/303.
[15] N.J. PETCH, The Cleavage Strength of Polycrystals, J. Iron Steel Inst. 174 (1953) 25–28.
[16] N. Hansen, Hall-Petch relation and boundary strengthening, Scr. Mater. 51 (2004) 801–806, doi:10.1016/j.scriptamat.2004.06.002.
[17] A.H. Chokshi, A. Rosen, J. Karch, H. Gleiter, On the validity of the hall-petch relationship in nanocrystalline materials, Scr. Metall. 23 (1989) 1679–1683, doi:10.1016/0036-9748(89)90342-6.
[18] J.E. Sanchez, E. Arzt, Effects of grain orientation on hillock formation and grain growth in aluminum films on silicon substrates, Scr. Metall. Mater. 27 (1992) 285–290, doi:10.1016/0956-716X(92)90513-E.
[19] R. Venkatraman, J.C. Bravman, Separation of film thickness and grain boundary strengthening effects in Al thin films on Si, J. Mater. Res. 7 (1992) 2040–2048, doi:10.1557/JMR.1992.2040.
[20] Z.C. Cordero, B.E. Knight, C.A. Schuh, Six decades of the Hall–Petch effect – a survey of grain-size strengthening studies on pure metals, Int. Mater. Rev. 61 (2016) 495–512, doi:10.1080/09506608.2016.1191808.
[21] A.R. Wildes, J. Mayer, K. Theis-Bröhl, The growth and structure of epitaxial niobium on sapphire, Thin Solid Films 401 (2001) 7–34, doi:10.1016/S0040-6090(01)01631-5.
[22] E.J. Grier, M.L. Jenkins, A.K. Petford-long, R.C.C. Ward, M.R. Wells, Misfit dislocations of epitaxial (110) niobium || (1120) sapphire interfaces grown by molecular beam epitaxy, Thin Solid Films 358 (2000) 94–98.
[23] G. Gutekunst, J. Mayer, M. Rühle, Atomic structure of epitaxial Nb-Al $_2$ O $_3$ interfaces I. Coherent regions, Philos. Mag. A. 75 (1997) 1329–1355, doi:10.1080/01418619708209859.
[24] G. Gutekunst, J. Mayer, V. Vitek, M. Rühle, Atomic structure of epitaxial Nb-Al $_2$ O $_3$ interfaces II. Misfit dislocations, Philos. Mag. A. 75 (1997) 1357–1382, doi:10.1080/01418619708209860.
[25] P. Klose, M. Hamm, V. Roddatis, A. Pundt, Influence of steel on the mechanical stress development during hydrogen-loading of ultrathin Nb-films, Int. J. Hydrogen Energy. 42 (2017) 22583–22588, doi:10.1016/J.IJHYDENE.2017.04.229.
[26] W. Zhang, S. Luo, T.B. Flanagan, Hydrogen solution in homogeneous Pd–Fe alloys, J. Alloys Compd. 293–295 (1999) 1–6, doi:10.1016/S0925-8388(99)00377-1.
[27] R. Kirchheim, R.B. McLellan, Electrochemical Methods for Measuring Diffusivities of Hydrogen in Palladium and Palladium Alloys, J. Electrochem. Soc. 127 (1980) 2419, doi:10.1149/1.2129486.
[28] J.M. Pureza, M.M. Lacerda, A.L. De Oliveira, J.F. Fragalli, R.A.S. Zanon, Enhancing accuracy to Stoney equation, Appl. Surf. Sci. 255 (2009) 6426–6428, doi:10.1016/j.apsusc.2009.01.097.
[29] N. Schwarzer, F. Richter, On the Determination of Film Stress from Substrate Bending: STONEY's Formula and Its Limits, Whitepaper (2006) 1–17 http://scholar.google.com/scholar?hl=en&btnG=Search&q=intitle:On+the+determination+of+film+stress+from+substrate+bending+:+S+TONEY+?+s+formula+and+its+limits#4.
[30] G.G. Stoney, The Tension of Metallic Films Deposited by Electrolysis, Proc. R. Soc. London. Ser. A, Contain. Pap. a Math. Phys 82 (1909) 172–175 Character http://www.jstor.org/stable/92886 .
[31] S. Wagner, P. Klose, V. Burlaka, K. Nörthemann, M. Hamm, A. Pundt, Structural Phase Transitions in Niobium Hydrogen Thin Films: Mechanical Stress, Phase Equilibria and Critical Temperatures, ChemPhysChem (2019) 20, doi:10.1002/cphc.201900247.
[32] P.F. Miceli, H. Zabel, J.A. Dura, C.P. Flynn, Anomalous lattice expansion of metal-hydrogen thin films, J. Mater. Res. 6 (1991) 964–968, doi:10.1557/JMR.1991.0964.
[33] T. Schober, H. Wenzl, in: The systems NbH(D), TaH(D), VH(D) : Structures, phase diagrams, morphologies, methods of preparation, Springer, Berlin, Heidelberg, 1978, pp. 11–71, doi:10.1007/3-540-08883-0_18.
[34] M. Choy, K. Hellwege, A. Hellwege, Elastic, piezoelectric, pyroelectric, piezooptic, electrooptic constants, and nonlinear dielectric susceptibilities of crystals, revised and expanded edition of (1979).
[35] U. Laudahn, S. Fahler, H.U. Krebs, A. Pundt, M. Bicker, U. Hülsen, U. Geyer, R. Kirchheim, Determination of elastic constants in thin films using hydrogen loading, Appl. Phys. Lett. 74 (1999) 647–649, doi:10.1063/1.123028.
[36] R.L. Barns, Niobium: Lattice Parameter and Density ARTICLES YOU MAY BE INTERESTED IN (2003), doi:10.1063/1.1656912.
[37] D. Sander, The correlation between mechanical stress and magnetic anisotropy in ultrathin films, Reports Prog. Phys. 62 (1999) 809–858, doi:10.1088/0034-4885/62/5/204.
[38] S. Wagner, P. Klose, V. Burlaka, K. Nörthemann, M. Hamm, A. Pundt, Structural Phase Transitions in Niobium Hydrogen Thin Films: Mechanical Stress, Phase Equilibria and Critical Temperatures, ChemPhysChem 20 (2019) 1890–1904, doi:10.1002/cphc.201900247.
[39] A. Kirchheim, R. Pundt, Hydrogen in Metals, Phys. Metall. (2014) 2597–2705.
[40] C. Lemier, J. Weissmüller, Grain boundary segregation, stress and stretch: Effects on hydrogen absorption in nanocrystalline palladium, Acta Mater 55 (2007) 1241–1254, doi:10.1016/j.actamat.2006.09.030.